Phage-display selection of a cell-permeable bicyclic peptide as a selective ligand of the human RNA decapping enzyme Dcp2

Yang Luo[†‡], Zhenkun Na[†‡] and Sarah A. Slavoff[†‡I*]

[†]Department of Chemistry, Yale University, New Haven, Connecticut 06520, United States

[‡]Chemical Biology Institute, Yale University, West Haven, Connecticut 06516, United States

[I]Department of Molecular Biophysics and Biochemistry, Yale University, New Haven, Connecticut 06529, United States

*Correspondence: sarah.slavoff@yale.edu

ABSTRACT: Dcp2 is an important enzyme that controls the stability of a subset of human cellular RNAs encoding functions such as transcription and immune responses. While >1800 Dcp2 substrates have been identified in human cells, compensatory gene expression changes secondary to genetic ablation of the *DCP2* gene have complicated a complete mapping of its regulome. Cell-permeable, selective chemical ligands of Dcp2 could facilitate development of improved tools for elucidation of its function and cellular specificity. Here, we report the selection of a bicyclic peptide ligand of human Dcp2 from chemically cyclized phage-encoded libraries, and evaluation of its affinity and selectivity for Dcp2 *in vitro* and in cells. Quantitative reverse transcription PCR (qRT-PCR) combined with a splinted ligation assay revealed that this stapled bicyclic peptide inhibits Dcp2 decapping activity toward specific RNA substrates inside human cells. We further demonstrate that CP21 increases formation of P-bodies, cellular liquid condensates enriched in intermediates of cellular RNA decay, in the same manner as deletion or mutation of Dcp2. Collectively, these results demonstrate development of a selective ligand of Dcp2 that modulates some of its functions inside cells. In the future, this molecule – and, more broadly, stapled peptide selection – may find utility in reverse chemical genetics to dissect the specificities of coexistent cellular RNA decay pathways.

INTRODUCTION

The first step of 5'-3' exonucleolytic RNA decay in eukaryotes is the removal of the 7-methylguanosine (m^7G) cap of deadenylated transcripts[1]. In yeast this is primarily accomplished by the Nudix family decapping enzyme Dcp2[2-6], under tight temporal and spatial regulation of decapping activator proteins such as Dcp1[1], post-translational modifications[7], and phase separation into liquid structures known as processing bodies (P-bodies)[8, 9]. However, the landscape of RNA decapping enzymes is more complex in mammals than in lower eukaryotes[10, 11]. Mammals encode multiple RNA m^7G decapping enzymes, including Nudt16[12, 13] and Nudt3[14], as well as Dxo/Rai1, which hydrolyzes both unmethylated[15, 16] and NAD caps[10, 17], suggesting that that Nudix family hydrolases could regulate different subsets of the transcriptome despite their lack of apparent *in vitro* sequence specificity[13]. While preliminary evidence for orthogonal regulation of targeted genes by Dcp2, Nudt16 and Nudt3 supports this hypothesis[12, 14, 18, 19], a complete global mapping of the cellular substrates of mammalian decapping enzymes has not yet been achieved.

Dcp2 controls the stability of a large but specific subset of human transcripts. We recently obtained global, time-resolved measurements of RNA dynamics to identify ~1800 transcripts that are stabilized in *DCP2* knockout (KO) cells, suggesting that they are Dcp2 substrates [Luo et al., manuscript accepted]. Considered together with prior studies, transcripts comprising the Dcp2 regulome have important properties including (1) regulatory and immune functions, (2) enrichment in P-bodies, and (3) modification with N^6-methyladenosine (m^6A). Nonetheless, we also observed a significant number of destabilized RNAs and transcriptional changes in *DCP2* KO cells, indicative of secondary changes as a result of genetic compensation for *DCP2* deletion and complicating comprehensive identification of Dcp2 targets. A more complete and accurate mapping of Dcp2 substrates may therefore require development of chemical genetic tools toward the goal of acute Dcp2 inhibition or depletion.

Structural characterization of complexes of yeast Dcp2 has revealed the mechanistic basis for catalysis and allosteric activation[20-25]. Dcp2 utilizes a bipartite active site, with critical residues contributed both by the Nudix domain and the distal N-terminal regulatory domain (NRD). Yeast Dcp1/human Dcp1a is a conserved activator of decapping, which contacts the Dcp2 NRD either through direct interaction with the Dcp1 EVH1 (Ena/VASP homology 1) domain in yeast[26] or through the scaffold protein EDC4 in higher eukaryotes[27, 28] to promote formation of a pre-catalytic closed conformation of Dcp2. Additional factors, such as yeast Edc1[20, 23, 24] and Edc3[25], release the autoinhibition by a C-terminal segment and correctly position residues critical for cap recognition and hydrolysis by Dcp2 in its active conformation. It is important to note that molecular details that regulate Dcp2 activity in human can be fundamentally different from yeast, especially with regard to

protein-protein interaction networks[27, 29]. Given the conformational flexibility of Dcp2, directly targeting the catalytic site with small-molecule inhibitors might be challenging[30]. Furthermore, Dcp2 has low affinity for small molecule cap analogs because it requires an intact capped RNA substrate of at least 12 residues[31], which can be difficult to prepare in large scale for *in vitro* ligand or inhibitor screening. These factors present significant challenges to development of inhibitors and ligands via small molecule design or screening.

Despite these challenges, Dcp2 inhibitors have been previously reported. These bivalent cap analogues, consisting of two m^7G moieties joined by a 5'-to-5' tetraphosphate bridge to increase binding affinity, have been reported to bind to and inhibit the active conformation of Dcp2 at the catalytic site[22, 30]. The D3 diastereomer of the most potent analog, bearing α- and δ-phosphorothiolate substitution, exhibited a K_i of 121±16 μM for *Schizosaccharomyces pombe* Dcp2 (spDcp2)[30]. Intriguingly, these inhibitors exhibit increased affinity toward the reconstituted spDcp1/2 complex compared to spDcp2 alone, making then particularly valuable for structural and mechanistic studies[22, 23]. However, membrane impermeability of these cap dinucleotide analogues and limited affinity may impair their utility for cellular studies. It is also unclear whether these cap analogues are selective toward Dcp2 versus other mammalian RNA decapping enzymes.

Recognizing the lack of a preformed, high affinity substrate binding pocket in Dcp2 for ligand or inhibitor binding, another approach is to target surface or allosteric sites, which we hypothesized could be achieved with proteomimetics[32]. Chemically stapled or cyclized peptides are emergent classes of ligands developed to target large protein surfaces inaccessible by small molecules[33-35]. Besides mimicking structured protein-binding domains, these molecules feature resistance to proteolytic degradation compared to their linear equivalents *in vivo*, as well as detectable membrane permeability when optimized[36, 37]. In 2009, Heinis *et al.* reported a phage-encoded stapled bicyclic peptide library that enables *in vitro* selection of ligands for protein targets[38]. Here, we apply this method to identify a cyclic peptide, CP21, which functions as a selective and cell-permeable human Dcp2 ligand. We also report the *in cellulo* effect of this peptide on the stability of previously reported Dcp2 target RNAs and on P-body formation. Overall, our data demonstrates CP21 as a highly selective ligand of Dcp2 *in vitro* and in cells that modulates the cellular activity of Dcp2.

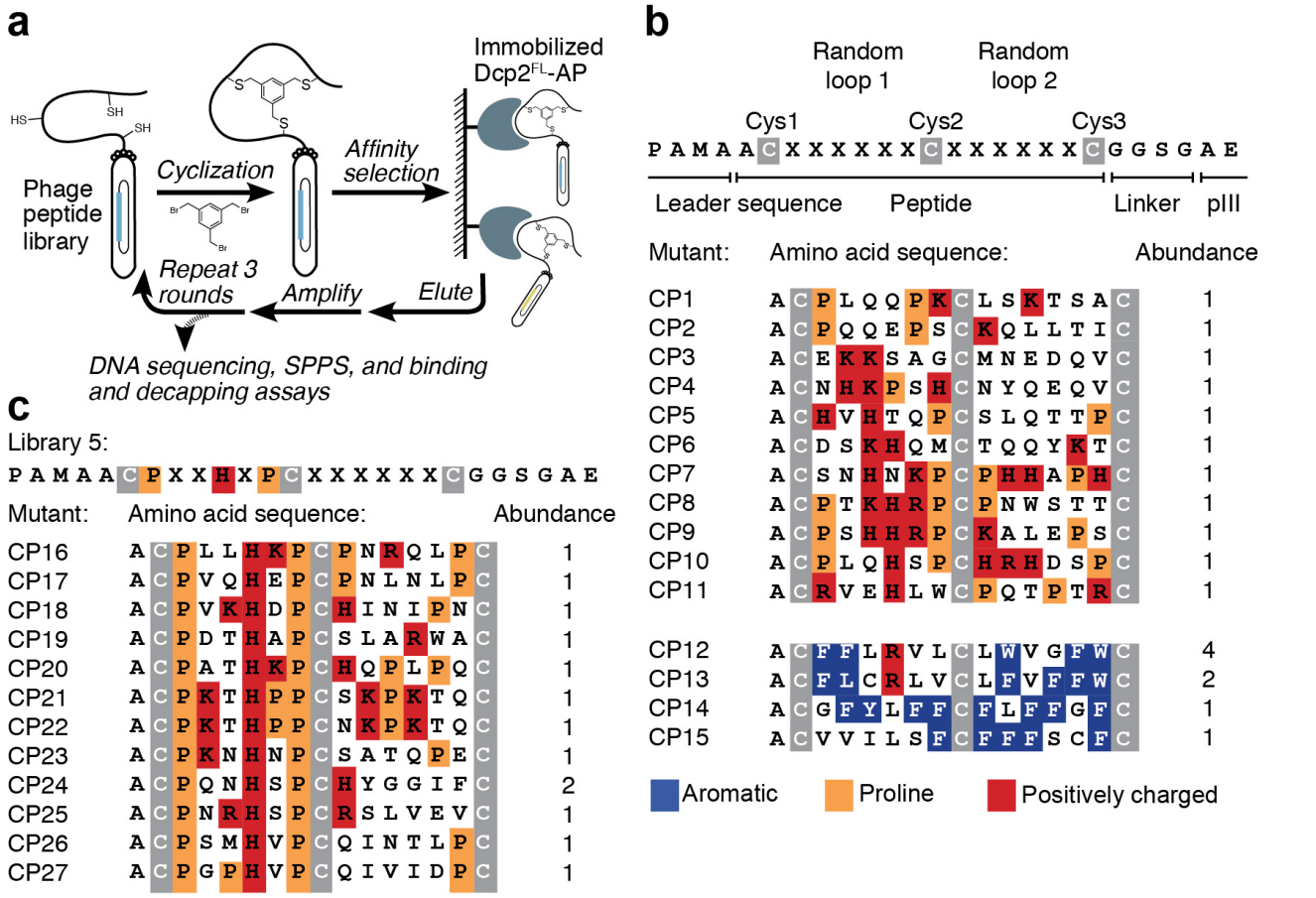

Figure 1. Phage display selection of bicyclic peptides that bind to human Dcp2 (Dcp2). (a) Schematic illustration of the strategy to select Dcp2 binders from a phage-displayed 6x6 peptide library containing 3 fixed cysteine residues for chemical cyclization with 1,3,5-tris(bromomethyl)benzene (TBMB). (b) Sequences of two classes of selected bicyclic peptides enriched by a site-specifically biotinylated Dcp2 construct, $Dcp2^{FL}$-AP (see Figure S1). Residues with aromatic side chains are highlighted in blue, positively charged residues red, and prolines orange. (c) Amino acid sequences of selected clones from affinity maturation with $Dcp2^{FL}$-AP. All clones derive from library 5, designed around the positively charged and proline-rich sequences enriched from the initial fully random library (b, top).

We propose that this peptide scaffold can in the future be further developed into chemical genetic tools useful in mapping the substrate specificity of human Dcp2, and that this general strategy may be broadly applicable to ligand development for other RNA decay enzymes toward chemical genetic dissection of their functions and specificities.

RESULTS

Phage display screening identifies CP21 as a ligand of human Dcp2

We hypothesized that chemically stapled bicyclic peptides might recognize Dcp2 by binding to a large surface of the protein, as previously reported for human urokinase-type plasminogen activator (uPA)[39]. The initial peptide library consisted of two fully randomized 6-mer peptide sequences flanked by a total of three cysteine residues displayed on a disulfide-free phage pIII protein and was chemically cyclized with 1,3,5-tris(bromomethyl)benzene (TBMB), as previously described[40] (Figure 1a). To avoid blocking any ligandable hotspots on Dcp2, we approached target immobilization with a site-specific biotinylation strategy[41]. In brief, the 15-amino acid BirA biotin ligase substrate, AviTag peptide[42], was appended to the C-terminus of full-length Dcp2 (Dcp2^{FL}-AP), and the tagged protein was labeled *in vitro* using purified BirA and biotin. Successful biotinylation was confirmed using a streptavidin pull-down assay (Figure S1a-c). Site-specifically biotinylated Dcp2^{FL}-AP was then immobilized on streptavidin beads for phage display selection. Starting with 10^{10} purified TBMB-modified phage particles, three rounds of selection were performed, with amplification and cyclization of enriched phage before the next round of selection. Stringency of selection was increased in the 2nd and the 3rd round by doubling the wash steps and decreasing the concentration of Dcp2^{FL}-AP to facilitate enrichment of high-affinity Dcp2 binders. A beads-only negative control was included in all steps to exclude non-specific streptavidin binding. 100 colonies were sequenced from the last round to yield two classes of sequences (Figure 1b): one was enriched in positively charged amino acids and showed preference for proline in the first and the last two positions in either loop; the second group of false positives were characterized by highly hydrophobic and aromatic residues arising from the fully randomized nature of the peptide library and likely represented aggregation and/or nonspecific binding. New affinity maturation libraries were then constructed to

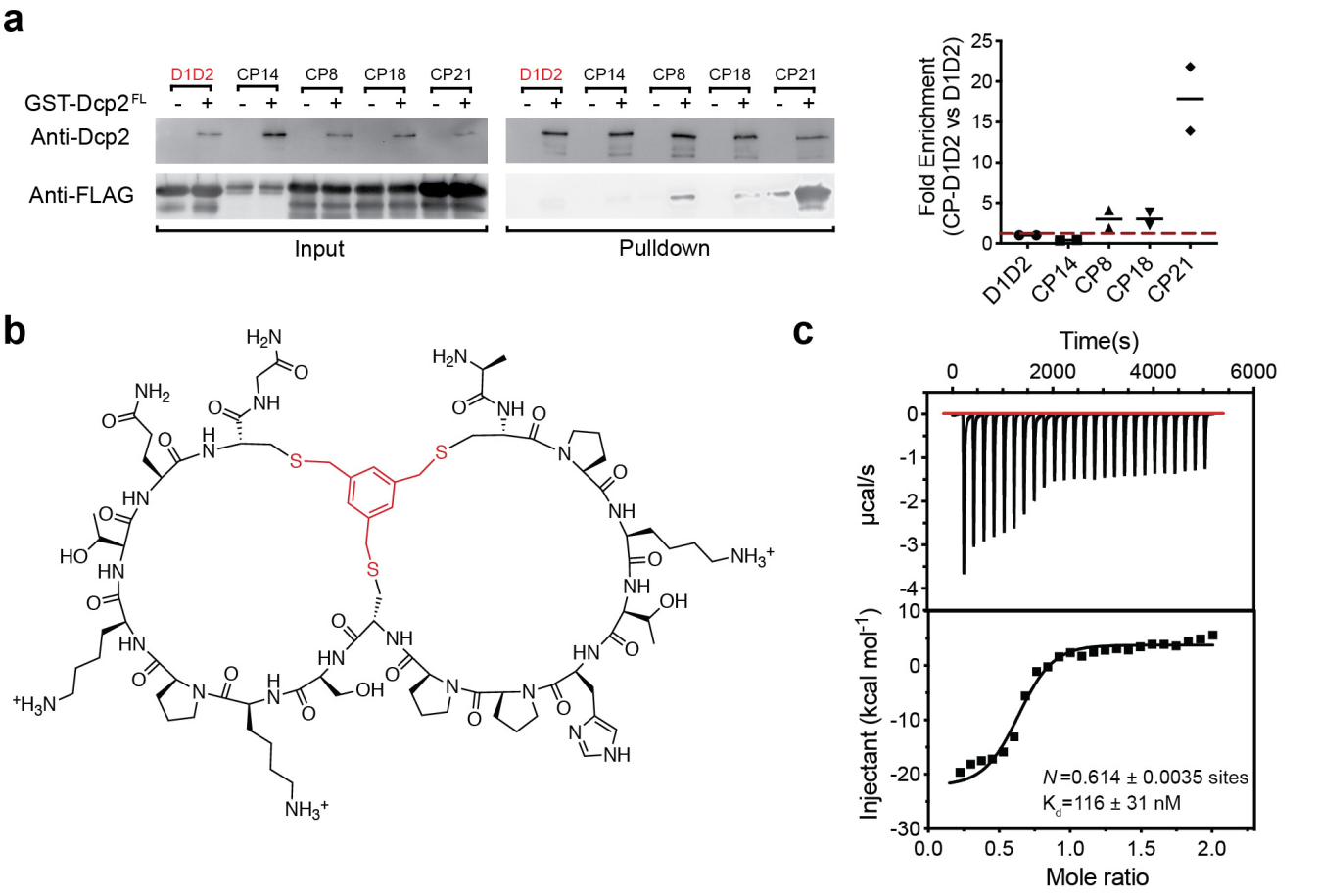

Figure 2. Cyclic peptide CP21 binds to Dcp2 *in vitro*. (a) Validation of Dcp2 binding to selected TBMB-cyclized peptides by *in vitro* pull-down assay. Phage-display-enriched CP sequences were selected and cloned as fusions to the cysteine-free D1D2 domain of phage pIII protein for bacterial expression, purified and chemically cyclized. GST-Dcp2^{FL} was co-incubated with 10-fold molar excess of the FLAG epitope-tagged CP-D1D2 fusion proteins, with D1D2 alone as a negative control, and GST pull-down was performed prior to western blot detection. Representative data of two technical replicates are shown. Lines from the scatter plot indicate the mean value of CP-D1D2 enrichment. (b) Chemical structure of CP21. (c) Isothermal calorimetry (ITC) of chemically synthesized CP21 binding to Dcp2$^{1\text{-}349}$. Data shown are representative of two technical replicates, and dissociation constant is reported as ± the error of fitting.

recapture the convergence in the first class by fixing consensus residue groups in one loop and leaving the rest randomized. The library was panned under stringent conditions (1 nM to 200 pM of $Dcp2^{FL}$-AP). Enriched peptides converged to a new consensus sequence (Figure 1c). Representative sequences from this selection were chosen for further characterization.

CP21 interacts with Dcp2 *in vitro*

While the affinity maturation revealed a new Dcp2 binding consensus, a single dominant sequence was not enriched, so we determined the best Dcp2 ligand through orthogonal *in vitro* binding assays. The DNA sequences of enriched peptides from both primary selection and affinity maturation were expressed, purified and TBMB-cyclized as peptide-D1D2-FLAG (disulfide-free phage protein pIII domains) fusion to test for their interaction with GST-$Dcp2^{FL}$ via a pull-down assay (Figure S1b,d). The best hit, CP21 (Figure 2a, b), which arose from affinity maturation, showed more than 15-fold higher enrichment of Dcp2 compared to the control (unfused D1D2 phage protein). CP21 peptide with an extra N-terminal alanine and C-terminal amidated glycine[38] was then chemically synthesized, cyclized with TBMB, purified by HPLC (high-performance liquid chromatography) and used for all following studies (Figure S2a). The K_d of synthetic CP21 for the catalytically active $Dcp2^{1-349}$ truncation construct[43] (Figure S1a,b) was 116 ± 31 nM by isothermal titration calorimetry (ITC) (Figure 2c). In contrast, the synthetic all-D enantiomeric form of CP21 (D-CP21, Figure S2b) showed undetectable binding to $Dcp2^{1-349}$ in ITC (Figure S3). In sum, these results support a specific association between CP21 and Dcp2.

CP21 contacts a C-terminus disordered segment of Dcp2

To understand the binding of CP21 to Dcp2, we used photo-cross-linking-based affinity enrichment and proteomics to confirm the physical interaction and to map sites potentially involved in the binding. To ensure efficient photo-cross-linking without disrupting Dcp2-CP21 interactions, we replaced residues unconserved in the most enriched peptide sequences from the phage display selection with photoreactive amino acids, L-Photo-Methionine (Photo-M) or L-Photo-Leucine (Photo-L), at either loops or near the cyclization center (Photo-CP-1 to -3, Figure S2c-e and Figure S4a). Biotin was added to

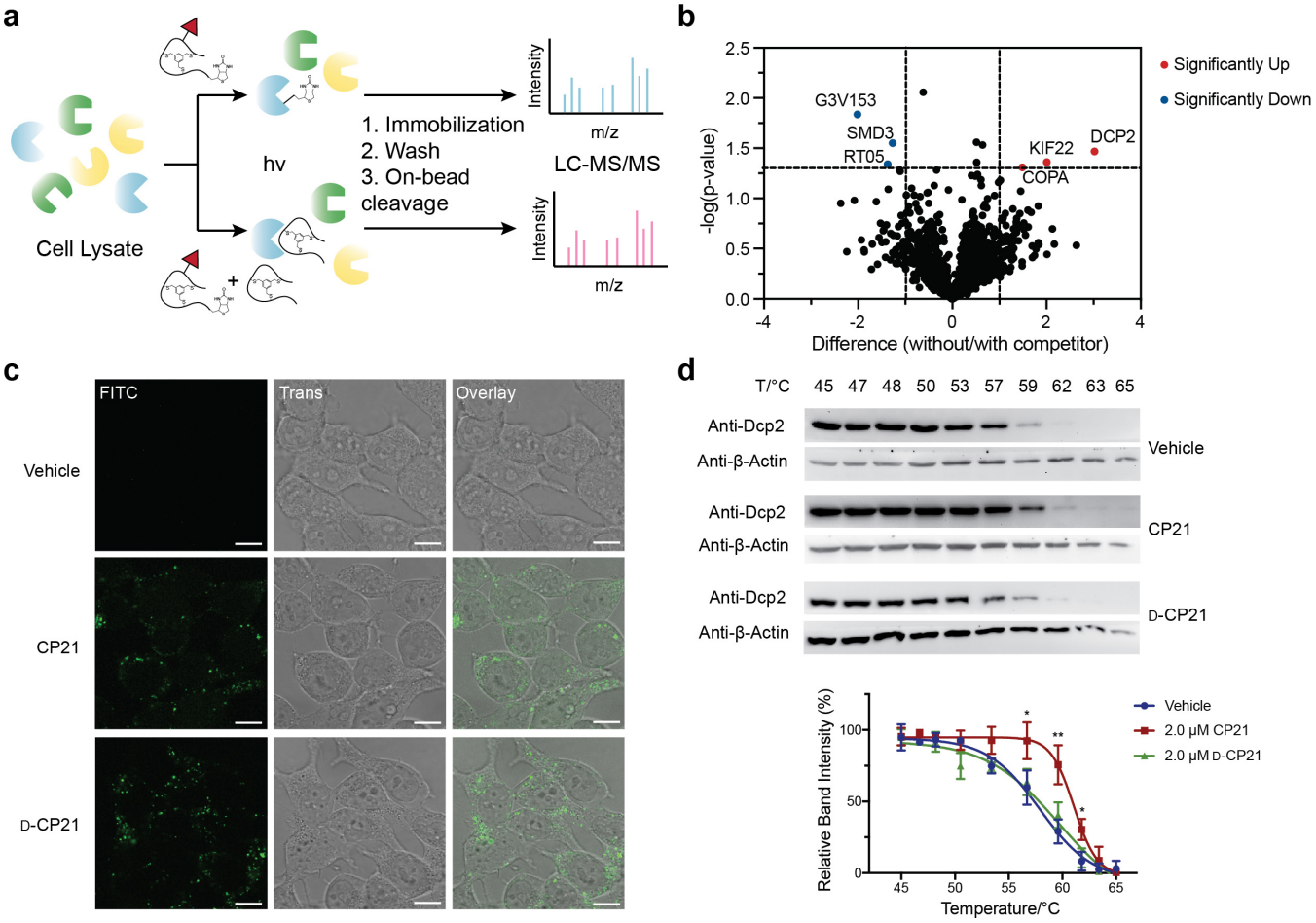

Figure 3. CP21 selectively binds to Dcp2 in cells. (a) Schematic representation of the target ID workflow. (b) Volcano plot of protein enrichment ratios (without/with 5-fold excess of unlabeled CP21 as competitor) and p-values from target ID experiments (n=3). (c) Assessment of cellular uptake of the cyclic peptides by live-cell confocal fluorescence microscopy of HEK293T cells incubated with vehicle or FITC-labeled CP21 in either all-L or all-D form (3 μM, 5 h). Z-plane scanning was performed to minimize signal from cell surface. Images are representative of two independent experiments. Scale bars, 10 μm. Trans, transillumination. (d) Cellular thermal shift assay (CETSA) of Dcp2 in the presence and absence of 2 μM CP21 in intact HEK293T cells. D-CP21 was used as a negative control. Significant differences in Dcp2 intensity (band densitometry) at 57, 59 and 62 °C were analyzed by one-way ANOVA. Number of biological repeats: n=3. Error bars represent ± s.d. P-values (with Dunnett's test) are denoted by asterisks; (*) $p<0.05$; (**) $p<0.01$.

the N-terminus of all peptides through an alkyl linker as an affinity handle for enrichment of interacting proteins. We assayed photo-cross-linking between each Photo-CP probe and purified $Dcp2^{1-349}$ and observed the most cross-linked product formation above background using Photo-CP-3 (Figure S4b). We next performed mass spectrometry analysis of pre- and post-photo-cross-linked samples. Dcp2 tryptic peptides reproducibly identified in at least 2 of 3 replicate non-cross-linked samples, but not detected in all replicate cross-linked samples, were identified as possibly involved in the binding of CP21 (Figure S4c). Three distinct putative cross-linking events occurred at or near the Nudix domain, while one was near the C-terminal FEB (phenylalanine-rich EDC4 binding) motif known to interact with EDC4, an important scaffolding protein of the active human decapping complex[27, 29].

Recent structural studies of yeast Dcp2 demonstrated the functional importance of intrinsically disordered regions[25], though the disordered C-terminus of human Dcp2 is distinct in sequence from that of yeast and has not been functionally characterized beyond the FEB motif. We therefore became interested in examining the role of the disordered C-terminal segment of human Dcp2 in CP21 binding. We generated alanine mutants of GST-tagged $Dcp2^{FL}$ between amino acids 325 and 333 and examined binding with CP21-D1D2-FLAG. Mutation of Q332 or K333 both caused ~50% reduction in the amount of $Dcp2^{FL}$ enriched from the pull-down compared to "wild type" CP21 (Figure S4d). These data support an involvement of the disordered C-terminal region in the binding between CP21 and Dcp2.

Dcp2 is the main cellular target of CP21

UV-mediated cross-linking combined with subsequent mass spectrometry is a powerful strategy for the identification of direct interactions between biological macromolecules in the cellular context[44]. To investigate the ability of CP21 to selectively engage Dcp2 over other cellular proteins and RNA decay factors, we proceeded to use Photo-CP-3 to examine a direct binding of CP21 to Dcp2 in whole cell lysates (Figure 3a). Incubation of Photo-CP-3 with HEK293T cell lysates overexpressing Dcp2 in the presence or absence of 5-fold excess of unlabeled CP21 as a competitor, followed by pull-down and quantitative proteomics, revealed enrichment of Dcp2 over all other proteins, supporting Dcp2 as the primary cellular target of CP21 (Figure 3b).

We then asked whether the CP21 peptide could penetrate the cell membrane and selectively bind to Dcp2 in the cytoplasm. N-terminally FITC-labeled CP21 with an aminohexanoic (Ahx) acid spacer was chemically synthesized, purified (Figure S2f, g) and its cellular uptake examined by live-cell fluorescence confocal microscopy. HEK293T cells incubated with FITC-Ahx-CP21 or the all-D enantiomer (3 μM, 5 h) exhibited comparable internalization (Figure 3c). While a majority of observed fluorescence was punctate, consistent with endosomal localization[37], the presence of a low level of diffuse cytoplasmic signal could be consistent with detectable endosomal escape. Cellular uptake of stapled peptides has previously been proposed to be a result of their stabilized conformations via cyclization[36, 45].

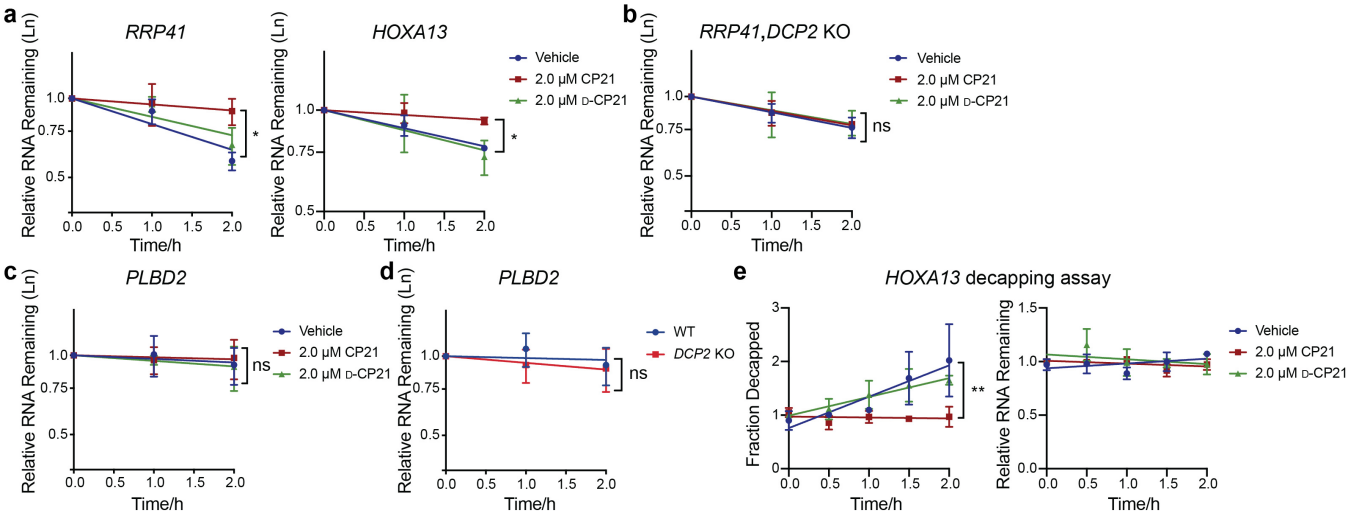

Figure 4. CP21 stabilizes specific cellular Dcp2 targets at the decapping step. (a) mRNA decay curves of known Dcp2 targets from HEK293T cells treated with 2 μM of CP21 (red), D-CP21 (green), or vehicle (equal volume of peptide storage buffer, blue). Relative levels of each mRNA remaining at indicated time points following actinomycin D treatment were determined by quantitative reverse transcription PCR (qRT-PCR, see methods). Error bars represent mean ± s.d. Number of biological repeats: n=3. Significance was derived from one-way ANOVA of the slope of regression lines; (*) $p<0.05$. (b) Decay of *RRP41* mRNA in *DCP2* KO HEK293T cells treated with CP21, D-CP21, or vehicle. Number of biological repeats: n=3. Error bars represent ± s.d. P-values (with Dunnett's test) are denoted by asterisks; (ns) non-significant. (c,d) *PLBD2*, the stability of which is not affected by Dcp2 (d), was not stabilized by CP21 according to qRT-PCR analysis (c). Number of biological repeats: n=3. Error bars represent ± s.d, and significance was evaluated with ANOVA (c) or t-test linear regression (d); (ns) non-significant. (e) Splinted ligation RT-PCR (qSL-RT-PCR) assay was used to detect decapped mRNA under CP21 treatment. The relative fraction decapped *HOXA13* transcripts following transcriptional block for the indicated times in *XRN1* KO cells treated with CP21, D-CP21, or vehicle was normalized to t = 0 (left). The mean of three biological replicates was plotted. Significance at all time points was analyzed by ANOVA linear regression. Error bars represent ± s.d. P-values (with Dunnett's test) are denoted by asterisks; (*) $p<0.05$; (**) $p<0.01$. Total RNA level of *HOXA13* in *XRN1* KO cells from the same samples measured by qRT-PCR suggested treatment with neither compound affects total RNA level in *XRN1* KO (right).

To further evaluate Dcp2-engagement of CP21 in the cytoplasm, cellular thermal shift assay (CETSA) was performed in HEK293T cells[46]. In comparison to the vehicle-treated group, the melting temperature of Dcp2 was increased by 3.2 °C when cells were treated with 2 μM CP21, while no significant difference was observed when cells were treated with D-CP21 (Figure 3d). Taken together with selective cross-linking of Photo-CP-3 to Dcp2 in whole cell lysates observed in the target ID experiment, these pieces of evidence are consistent with selective CP21 binding to Dcp2 in cells.

CP21 modulates stability of selected Dcp2 targets at the decapping step

We investigated the activity and specificity of CP21 toward Dcp2 activity inside cells by measuring the transcript levels of endogenous reporter genes using qRT-PCR. Previously, Kiledjian and coworkers reported *RRP41* RNA as a preferred substrate of human Dcp2[19]. More recently, we demonstrated that *HOXA13* RNA is a Dcp2 target [Luo et al., manuscript accepted]. We thus used these two transcripts as endogenous reporters to evaluate the effect of CP21 on Dcp2. Briefly, cells were pre-treated with CP21 and controls, then transcription was inhibited with actinomycin D and RNA levels assessed at specified timepoints to measure decay. Both RNAs were significantly stabilized by CP21 (2 μM) compared to controls (vehicle or D-CP21) (Figure 4a). Importantly, the same effect was observed for the K333A mutant of Dcp2 (which abrogates CP21 binding) when this mutant was expressed on a *DCP2* KO background in HEK293T cells (Figure S5a-b), demonstrating that this mutation phenocopies CP21 treatment, and furthermore providing the first demonstration that this mutation in the disordered C-terminal region inhibits Dcp2 activity. The fact that D-CP21 did not alter the stability of either RNA indicates that the observed inhibition of RNA decay was specific to inhibitory activity of CP21 in its all-L form. Importantly, we found that CP21 did not lead to a further increase in the stability of the *RRP41* transcript in the *DCP2* KO cell line, suggesting that CP21 mediates its *RRP41*-stabilizing effect specifically through Dcp2 and not via off-target inhibition or other non-specific effects (Figure 4b). Stability of a non-Dcp2 target RNA, *PLBD2*, remained unchanged by CP21 treatment (Figure 4c-d), further supporting a specific effect on Dcp2-mediated decay pathways.

Because these cell-based RNA stability assays provide indirect readouts of Dcp2 activity and inhibition, we required a direct measurement of RNA decapping in cells. We utilized a splinted ligation assay to quantify decapped RNA, which accumulates to detectable concentrations in yeast or mammalian cells lacking the downstream exonuclease Xrn1[47] [Luo et al., manuscript accepted]. In brief, sequence-specific enzymatic ligation of decapped RNA, which bears a 5'-phosphate group[47], was mediated by a DNA splint bridging an anchor RNA oligonucleotide of known sequence and 5' UTR of the target transcript, allowing quantitation of fractional decapped product relative to total RNA via qRT-PCR. *HOXA13* was selected as the reporter in this assay, and its decapping in *XRN1* KO cells treated with 2 μM CP21, D-CP21 or vehicle was measured (Figure 4e). The transient accumulation of decapped *HOXA13* was specifically abolished in CP21-treated cells. In sum, these data suggest that CP21 stabilize RNAs through specific modulation of Dcp2 decapping activity in cells.

CP21 induces the formation of phase separated RNA-decay foci

CP21-mediated modulation of Dcp2 might be expected to phenocopy genetic knockout, silencing or inactivating mutation of Dcp2. P-bodies are cytoplasmic liquid domains enriched in translationally repressed RNAs in complex with RNA decay-associated proteins[8, 48]. Deletion or silencing of Dcp2 has been shown to increase P-body numbers in yeast[49] and mammalian cells[50], possibly due to accumulation of deadenylated RNA decay intermediates in complex with proteins that can phase separate at high local concentrations. We observed that expression of the Dcp2 K333A mutant (on the *DCP2* KO background) caused a statistically significant 1.3-fold increase in P-body numbers relative to expression of wild type Dcp2, consistent with Dcp2 inhibition (Figure S5c). We thus asked whether CP21 treatment would affect P-body numbers. Indeed, CP21 increased P-body numbers compared to vehicle-treated cells (Figure 5), with 2.3 foci and 1.6 foci per cell, respectively, on average, while P-body numbers in D-CP21 treated cells remained unaltered (1.5 foci per cell). Taken together, our RNA stability and P-body imaging data suggest that CP21 modulates the cellular function of Dcp2.

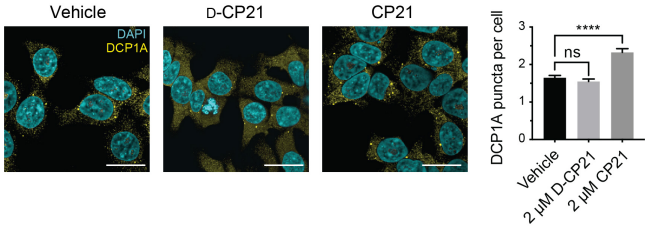

Figure 5. P-body numbers in HEK293T cells treated with CP21, D-CP21, or vehicle. Fixed cells were stained with antibodies detecting DCP1A, a P-body marker. Six fields of view (≥ 180 cells) were used to quantitate average P-bodies per cell in each condition. P-body numbers were counted using ImageJ as previously described (Nissan, T. and Parker R., 2008). Data represent mean values ± s.e.m, and significance was evaluated with one-way ANOVA. P-values (with Dunnett's test) are denoted by asterisks; (ns) non-significant, (****) $p<0.0001$. Scale bars, 25 μm.

DISCUSSION

In this work, we present the selection of CP21 as a cell-permeable bicyclic peptide modulator of Dcp2 activity. Importantly, the observed selectivity of CP21 to Dcp2 over other cellular proteins, including related RNA binding proteins and decapping enzymes, renders it a promising building block for chemical genetic strategies to probe Dcp2 in cells. The specificity of CP21 for Dcp2 binding and modulation is further supported by the inactivity of its enantiomer, D-CP21. Unexpectedly, in addition to the Nudix domain, a C-terminal disordered region of Dcp2 may be involved in its binding with CP21. We demonstrate the importance of this region in human Dcp2 for the first time, by showing that Dcp2 target decay rates are slowed and P-bodies are increased by the K333A Dcp2 mutant. While further work will be needed to fully elucidate the function of the human Dcp2 C-terminus, the mode of binding of CP21 to Dcp2 and the involvement of two distal regions of the protein in this binding, we suggest that this feature could potentially explain the outstanding selectivity of CP21 for Dcp2 and open new opportunities for understanding the mechanism of human Dcp2 activation. However, we note that, in contrast to the target-specific RNA decay assays reported in this work, CP21 has only a small effect on global RNA stability (data not shown), suggesting that it has not yet been optimized for use in

Dcp2 inhibition and substrate profiling. The mechanism by which CP21 modulates the stabilities of specific Dcp2 substrates therefore remains to be elucidated.

A significant increase in cellular P-body numbers was observed with CP21 treatment, phenocopying the effects of perturbed RNA decay at or after decapping on P-body abundance and size based on prior reports[49] and the K333A Dcp2 mutant (Figure S5c). Further supporting the dependence of this effect on Dcp2 binding, D-CP21 had no detectable effect on P-bodies. Additional experiments will be required to determine if the alteration of P-body numbers by CP21 is a cause or consequence of its modulation of Dcp2 activity; for example, the increase in P-bodies could be a result of the accumulation of deadenylated RNA promoting phase separation, or it could be an outcome of CP21-promoted changes in interactions between P-body components.

This study reports a selective Dcp2 ligand that can be used to modulate the decay of selected Dcp2 target transcripts and membraneless organelle formation, and unexpectedly identified a functional role for the disordered C-terminal region of human Dcp2. However, CP21 is not yet applicable to effective cellular inhibition of Dcp2 because its global effect on RNA stability remains limited. This is perhaps unsurprising, because CP21 was selected for Dcp2 binding, not inhibition. It is furthermore likely that CP21 is not optimally membrane permeable, leading to low effective concentration of the inhibitor within the cytosol. It is currently challenging to determine if Dcp2 is fully bound at the experimental CP21 concentration. Future efforts that focus on further biochemical and structural characterization of the Dcp2-CP21 interaction; determination of the effect of CP21 on Dcp2 structure, interactions, and activity in cells; and improving the cellular uptake of CP21 would address these issues. Should CP21 be found to be a Dcp2 ligand but not an efficient inhibitor, it could find utility in the context of a Dcp2 proteolysis targeting chimera (PROTAC). The selectivity of the Dcp2-CP21 interaction demonstrates that cyclic peptides could find broader use as building blocks for chemical genetic tools to bind, enrich, and modulate the activities of RNA decay factors.

ASSOCIATED CONTENT

Supporting Information

The Supporting Information is available free of charge on the ACS Publications website.

Experimental details and supplementary figures (PDF)
Proteomics data for target ID (XLSX)

AUTHOR INFORMATION

Corresponding Author

* E-mail: sarah.slavoff@yale.edu

Author Contributions

Y.L. designed and performed experiments and data analysis and wrote the manuscript. Z.N. generated the *XRN1* KO cell line and performed mass spectrometry experiments. S.A.S conceived the project, designed experiments and edited the manuscript. All authors have given approval to the final version of the manuscript.

Funding Sources

This work was supported in part by the NIH (R01GM122984), the Searle Scholars Program, and Yale University West Campus start-up funds (to S.A.S.).

ACKNOWLEDGMENT

We thank Dr. Christian Heinis (Institute of Chemical Sciences and Engineering, Ecole Polytechnique Fédérale de Lausanne, Lausanne, CH) for providing phage vectors (fdg3p0ss21 and fd0D12) and expert advice. We thank all members of the Slavoff lab for helpful discussion and comments on the manuscript. We also thank Prof. J. Ellman, A. Saghatelian, M. Simon and J. Crawford for valuable suggestions on the project.

REFERENCES

1. Li, Y.; Kiledjian, M., Regulation of mRNA decapping. *Wiley Interdiscip. Rev. RNA* **2010,** *1* (2), 253-65.
2. Dunckley, T.; Parker, R., The DCP2 protein is required for mRNA decapping in Saccharomyces cerevisiae and contains a functional MutT motif. *EMBO J.* **1999,** *18* (19), 5411-22.
3. Wang, Z.; Jiao, X.; Carr-Schmid, A.; Kiledjian, M., The hDcp2 protein is a mammalian mRNA decapping enzyme. *Proc. Natl. Acad. Sci. U. S. A.* **2002,** *99* (20), 12663-8.
4. Xu, J.; Yang, J. Y.; Niu, Q. W.; Chua, N. H., Arabidopsis DCP2, DCP1, and VARICOSE form a decapping complex required for postembryonic development. *Plant Cell* **2006,** *18* (12), 3386-98.
5. Behm-Ansmant, I.; Rehwinkel, J.; Doerks, T.; Stark, A.; Bork, P.; Izaurralde, E., mRNA degradation by miRNAs and GW182 requires both CCR4:NOT deadenylase and DCP1:DCP2 decapping complexes. *Genes Dev.* **2006,** *20* (14), 1885-98.
6. Lykke-Andersen, J., Identification of a human decapping complex associated with hUpf proteins in nonsense-mediated decay. *Mol. Cell. Biol.* **2002,** *22* (23), 8114-21.
7. Yoon, J. H.; Choi, E. J.; Parker, R., Dcp2 phosphorylation by Ste20 modulates stress granule assembly and mRNA decay in Saccharomyces cerevisiae. *J. Cell. Biol.* **2010,** *189* (5), 813-27.
8. Luo, Y.; Na, Z.; Slavoff, S., P-Bodies: Composition, Properties, and Functions. *Biochemistry* **2018,** *57* (17), 2424-2431.
9. Mugridge, J. S.; Coller, J.; Gross, J. D., Structural and molecular mechanisms for the control of eukaryotic 5'-3' mRNA decay. *Nat. Struct. Mol. Biol.* **2018,** *25* (12), 1077-1085.
10. Grudzien-Nogalska, E.; Kiledjian, M., New insights into decapping enzymes and selective mRNA decay. *Wiley Interdiscip. Rev. RNA* **2017,** *8* (1), e1379.
11. Kiledjian, M., Eukaryotic RNA 5'-End NAD. *Trends Cell Biol.* **2018,** *28* (6), 454-464.
12. Li, Y.; Song, M.; Kiledjian, M., Differential utilization of decapping enzymes in mammalian mRNA decay pathways. *RNA* **2011,** *17* (3), 419-28.
13. Song, M. G.; Li, Y.; Kiledjian, M., Multiple mRNA decapping enzymes in mammalian cells. *Mol. Cell* **2010,** *40* (3), 423-32.
14. Grudzien-Nogalska, E.; Jiao, X.; Song, M. G.; Hart, R. P.; Kiledjian, M., Nudt3 is an mRNA decapping enzyme that modulates cell migration. *RNA* **2016,** *22* (5), 773-81.
15. Jiao, X.; Chang, J. H.; Kilic, T.; Tong, L.; Kiledjian, M., A mammalian pre-mRNA 5' end capping quality control mechanism and an unexpected link of capping to pre-mRNA processing. *Mol. Cell* **2013,** *50* (1), 104-15.
16. Chang, J. H.; Jiao, X.; Chiba, K.; Oh, C.; Martin, C. E.; Kiledjian, M.; Tong, L., Dxo1 is a new type of eukaryotic enzyme with both decapping and 5'-3' exoribonuclease activity. *Nat. Struct. Mol. Biol.* **2012,** *19* (10), 1011-7.
17. Jiao, X.; Doamekpor, S. K.; Bird, J. G.; Nickels, B. E.; Tong, L.; Hart, R. P.; Kiledjian, M., 5' End Nicotinamide Adenine Dinucleotide Cap in Human Cells Promotes RNA Decay through DXO-Mediated deNADding. *Cell* **2017,** *168* (6), 1015-1027.e10.
18. Cohen, L. S.; Mikhli, C.; Jiao, X.; Kiledjian, M.; Kunkel, G.; Davis, R. E., Dcp2 Decaps m2,2,7GpppN-capped RNAs, and its

activity is sequence and context dependent. *Mol. Cell. Biol.* **2005,** *25* (20), 8779-91.

19. Li, Y.; Song, M. G.; Kiledjian, M., Transcript-specific decapping and regulated stability by the human Dcp2 decapping protein. *Mol. Cell. Biol.* **2008,** *28* (3), 939-48.

20. Valkov, E.; Muthukumar, S.; Chang, C. T.; Jonas, S.; Weichenrieder, O.; Izaurralde, E., Structure of the Dcp2-Dcp1 mRNA-decapping complex in the activated conformation. *Nat. Struct. Mol. Biol.* **2016,** *23* (6), 574-9.

21. Charenton, C.; Taverniti, V.; Gaudon-Plesse, C.; Back, R.; Séraphin, B.; Graille, M., Structure of the active form of Dcp1-Dcp2 decapping enzyme bound to m7GDP and its Edc3 activator. *Nat. Struct. Mol. Biol.* **2016,** *23* (11), 982-986.

22. Mugridge, J. S.; Ziemniak, M.; Jemielity, J.; Gross, J. D., Structural basis of mRNA-cap recognition by Dcp1-Dcp2. *Nat. Struct. Mol. Biol.* **2016,** *23* (11), 987-994.

23. Mugridge, J. S.; Tibble, R. W.; Ziemniak, M.; Jemielity, J.; Gross, J. D., Structure of the activated Edc1-Dcp1-Dcp2-Edc3 mRNA decapping complex with substrate analog poised for catalysis. *Nat. Commun.* **2018,** *9* (1), 1152.

24. Wurm, J. P.; Holdermann, I.; Overbeck, J. H.; Mayer, P. H. O.; Sprangers, R., Changes in conformational equilibria regulate the activity of the Dcp2 decapping enzyme. *Proc. Natl. Acad. Sci. U. S. A.* **2017,** *114* (23), 6034-6039.

25. Paquette, D. R.; Tibble, R. W.; Daifuku, T. S.; Gross, J. D., Control of mRNA decapping by autoinhibition. *Nucleic Acids Res.* **2018,** *46* (12), 6318-6329.

26. She, M.; Decker, C. J.; Svergun, D. I.; Round, A.; Chen, N.; Muhlrad, D.; Parker, R.; Song, H., Structural basis of dcp2 recognition and activation by dcp1. *Mol. Cell* **2008,** *29* (3), 337-49.

27. Chang, C. T.; Bercovich, N.; Loh, B.; Jonas, S.; Izaurralde, E., The activation of the decapping enzyme DCP2 by DCP1 occurs on the EDC4 scaffold and involves a conserved loop in DCP1. *Nucleic Acids Res.* **2014,** *42* (8), 5217-33.

28. Tritschler, F.; Braun, J. E.; Motz, C.; Igreja, C.; Haas, G.; Truffault, V.; Izaurralde, E.; Weichenrieder, O., DCP1 forms asymmetric trimers to assemble into active mRNA decapping complexes in metazoa. *Proc. Natl. Acad. Sci. U. S. A.* **2009,** *106* (51), 21591-6.

29. Chang, C. T.; Muthukumar, S.; Weber, R.; Levdansky, Y.; Chen, Y.; Bhandari, D.; Igreja, C.; Wohlbold, L.; Valkov, E.; Izaurralde, E., A low-complexity region in human XRN1 directly recruits deadenylation and decapping factors in 5'-3' messenger RNA decay. *Nucleic Acids Res.* **2019**, *47* (17), 9282-9295.

30. Ziemniak, M.; Mugridge, J. S.; Kowalska, J.; Rhoads, R. E.; Gross, J. D.; Jemielity, J., Two-headed tetraphosphate cap analogs are inhibitors of the Dcp1/2 RNA decapping complex. *RNA* **2016,** *22* (4), 518-29.

31. Arribas-Layton, M.; Wu, D.; Lykke-Andersen, J.; Song, H., Structural and functional control of the eukaryotic mRNA decapping machinery. *Biochim. Biophys. Acta* **2013,** *1829* (6-7), 580-9.

32. Horne, W. S.; Grossmann, T. N., Proteomimetics as protein-inspired scaffolds with defined tertiary folding patterns. *Nat. Chem.* **2020,** *12* (4), 331-337.

33. Walensky, L. D.; Bird, G. H., Hydrocarbon-stapled peptides: principles, practice, and progress. *J. Med. Chem.* **2014,** *57* (15), 6275-88.

34. Deyle, K.; Kong, X. D.; Heinis, C., Phage Selection of Cyclic Peptides for Application in Research and Drug Development. *Acc. Chem. Res.* **2017,** *50* (8), 1866-1874.

35. Vinogradov, A. A.; Yin, Y.; Suga, H., Macrocyclic Peptides as Drug Candidates: Recent Progress and Remaining Challenges. *J. Am. Chem. Soc.* **2019,** *141* (10), 4167-4181.

36. Dietrich, L.; Rathmer, B.; Ewan, K.; Bange, T.; Heinrichs, S.; Dale, T. C.; Schade, D.; Grossmann, T. N., Cell Permeable Stapled Peptide Inhibitor of Wnt Signaling that Targets β-Catenin Protein-Protein Interactions. *Cell Chem. Biol.* **2017,** *24* (8), 958-968.e5.

37. LaRochelle, J. R.; Cobb, G. B.; Steinauer, A.; Rhoades, E.; Schepartz, A., Fluorescence correlation spectroscopy reveals highly efficient cytosolic delivery of certain penta-arg proteins and stapled peptides. *J. Am. Chem. Soc.* **2015,** *137* (7), 2536-2541.

38. Heinis, C.; Rutherford, T.; Freund, S.; Winter, G., Phage-encoded combinatorial chemical libraries based on bicyclic peptides. *Nat. Chem. Biol.* **2009,** *5* (7), 502-7.

39. Angelini, A.; Cendron, L.; Chen, S.; Touati, J.; Winter, G.; Zanotti, G.; Heinis, C., Bicyclic peptide inhibitor reveals large contact interface with a protease target. *ACS Chem. Biol.* **2012,** *7* (5), 817-21.

40. Rentero Rebollo, I.; Heinis, C., Phage selection of bicyclic peptides. *Methods* **2013,** *60* (1), 46-54.

41. Fairhead, M.; Howarth, M., Site-specific biotinylation of purified proteins using BirA. *Methods Mol. Biol.* **2015,** *1266*, 171-84.

42. Schatz, P. J., Use of peptide libraries to map the substrate specificity of a peptide-modifying enzyme: a 13 residue consensus peptide specifies biotinylation in Escherichia coli. *Biotechnology (N Y)* **1993,** *11* (10), 1138-43.

43. Piccirillo, C.; Khanna, R.; Kiledjian, M., Functional characterization of the mammalian mRNA decapping enzyme hDcp2. *RNA* **2003,** *9* (9), 1138-47.

44. Pham, N. D.; Parker, R. B.; Kohler, J. J., Photocrosslinking approaches to interactome mapping. *Curr. Opin. Chem. Biol.* **2013,** *17* (1), 90-101.

45. Chu, Q.; Moellering, R.; Hilinski, G.; Kim, Y.; Grossmann, T.; Yeh, J.; Verdine, G., Towards understanding cell penetration by stapled peptides. *MedChemComm* **2015,** *6* (1), 111-119.

46. Jafari, R.; Almqvist, H.; Axelsson, H.; Ignatushchenko, M.; Lundbäck, T.; Nordlund, P.; Martinez Molina, D., The cellular thermal shift assay for evaluating drug target interactions in cells. *Nat. Protoc.* **2014,** *9* (9), 2100-22.

47. Blewett, N.; Coller, J.; Goldstrohm, A., A quantitative assay for measuring mRNA decapping by splinted ligation reverse transcription polymerase chain reaction: qSL-RT-PCR. *RNA* **2011,** *17* (3), 535-43.

48. Eulalio, A.; Behm-Ansmant, I.; Izaurralde, E., P bodies: at the crossroads of post-transcriptional pathways. *Nat. Rev. Mol. Cell Biol.* **2007,** *8* (1), 9-22.

49. Parker, R., Decapping and Decay of messenger rna occur in cytoplasmic processing bodies. *Science* **2003**, *300* (5620), 805-8.

50. Aizer, A.; Kalo, A.; Kafri, P.; Shraga, A.; Ben-Yishay, R.; Jacob, A.; Kinor, N.; Shav-Tal, Y., Quantifying mRNA targeting to P-bodies in living human cells reveals their dual role in mRNA decay and storage. *J. Cell. Sci.* **2014,** *127* (Pt 20), 4443-56.

TABLE OF CONTENTS GRAPHICS